Available online at www.sciencedirect.com
ScienceDirect
Trans. Nonferrous Met. Soc. China 34(2024) 3029−3041
Transactions of Nonferrous Metals Society of China
www.tnmsc.cn

Interphase migration and enrichment of lead and zinc during copper slag depletion

Jun HAO[1,2#], Zhi-he DOU[1,2#], Xing-yuan WAN[1,2], Ting-an ZHANG[1,2], Kun WANG[1,2]

1. Key Laboratory of Ecological Metallurgy of Multi-metal Intergrown Ores of Education, Northeastern University, Shenyang 110819, China;
2. School of Metallurgy, Northeastern University, Shenyang 110819, China

Received 27 March 2023; accepted 29 January 2024

Abstract: An interphase migration and enrichment model of lead and zinc during molten copper slag depletion was established. The occurrence of various components in copper slag was predicted using sulfur−oxygen potential calculations and confirmed through high-temperature experiments. The recovery rate of copper can reach 90.13% under the optimal conditions of 1200 °C, an iron to silicon mass ratio of 1.0, 3 wt.% ferrous sulfide, and a duration of 45 min. Lead (54.07 wt.%) and zinc (17.42 wt.%) are found in the flue dust as lead sulfate, lead sulfide, and zinc oxide, while copper matte contains lead (14.44 wt.%) and zinc sulfide (1.29 wt.%). The remaining lead and zinc are encapsulated as oxides within the fayalite phase.

Key words: depletion; lead; copper slag; stirring; zinc

1 Introduction

Copper slag is an industrial solid waste generated in the copper smelting and refining processes [1]. The production of copper slag is 2−3 times that of refined copper [2]. According to statistical data, the cumulative production of copper slag worldwide since 1999 has exceeded 752 million tons [3]. Copper smelters need to continuously enhance the oxygen potential in the copper smelting process to increase production capacity and meet supply-demand requirements [4]. This results in the copper content of most copper slag being even higher than that of copper ore, which has the lowest industrially exploitable grade (0.4 wt.%). Due to economic growth and population expansion, there will be a significant increase in the worldwide demand for resources in the coming decades [5,6]. The production of copper slag is projected to reach 6−9 times the current level by 2050 [7]. However, open-air stacking is the most prevalent method for handling copper slag [8], giving rise to numerous safety concerns [9,10]. As a result of precipitation [11] and physical, chemical, and biological weathering processes [12], heavy metals in copper slag can pose varying degrees of harm to the environment and individuals [13,14]. Hence, the efficient and environmentally friendly utilization of copper slag holds potential to ensure the environmentally sustainable development of the copper smelting industry [15].

The copper and iron contents in copper slag ranging from 0.58 to 2.71 wt.% and 31.70 to 40.31 wt.%, respectively [2]. Flotation, reduction-magnetic separation, and depletion are the primary

[#]Jun HAO and Zhi-he DOU contributed equally to this work

Corresponding author: Zhi-he DOU, Tel: +86-24-83686283, E-mail: douzh@smm.neu.edu.cn;
Ting-an ZHANG, Tel: +86-24-83686283, E-mail: zhangta@smm.neu.edu.cn

DOI: 10.1016/S1003-6326(24)66593-3

methods for recovering copper and iron resources from copper slag [16]. WANG et al [17] employed mechanical activation-enhanced flotation to recover copper from copper slag. Under the optimal flotation conditions of 600 g/t sodium carbonate and 300 g/t xanthate, the copper recovery rate reached 98.07%, achieving a copper concentrate grade of 36.13 wt.%. Consequently, the flotation process offers the advantages of high-purity concentrate and valuable metal recovery. However, it necessitates using finer mineral particle sizes and numerous flotation reagents, making it challenging to mitigate issues related to the wastewater treatment [18]. LI et al [19] investigated the reduction and magnetic separation of copper slag using sodium carbonate and calcium oxide as alkalinity regulators. With an alkalinity level of 0.5 and the addition of 8 wt.% sodium carbonate, the recovery rates for copper and iron reached 86.5% and 94.3%, respectively. The grades of the copper and iron concentrates reached 1.2 wt.% and 90.5 wt.%, respectively. The reduction magnetic separation method is effective in separating and recycling of copper and iron from copper slag [20]. However, the iron concentrate obtained through magnetic separation contains copper and cannot be directly used as a steelmaking raw material. Hence, achieving the synergistic recovery of copper and iron from copper slag necessitates a minimization in the copper content prior to iron recovery. WANG et al [21] implemented a high-gravity field in the copper slag depletion process. The results revealed that 97.98% copper in copper slag could be recovered in 5 min under a high gravity field at 1250−1300 °C. However, realizing a large-scale industrial expansion of high-gravity equipment will be extremely difficult. Research on the extraction of valuable components, such as lead and zinc, from copper slag is predominantly manifested in the leaching process. High leaching rates and selective element separation are achievable through leaching for copper slag [22]. However, it is imperative to address the challenges related to acid mist, pipeline erosion, and acid wastewater in the production process [23].

The concept of latent heat of copper slag (LHOCS) is a relatively recent and underexplored subject that has received limited attention in previous scholarly research. Currently, the raw materials employed for the resource utilization of copper slag are mainly cold copper slag, derived from hot molten copper slag at temperatures of 1150−1250 °C. The thermal energy carried by the molten copper slag is called LHOCS. The LHOCS is challenging to utilize effectively in the current industrial processes. About 80% of global copper is produced using pyrometallurgical technology, which will generate a large amount of molten copper slag carrying LHOCS. Based on the data on global copper slag production in 2022, it is estimated that inadequate utilization of LHOCS has led to an economic loss of approximately 2×10^{10} CNY. The lead and zinc contents in the collected flue dust from copper slag range from 0.1−0.4 wt.% to 0.9−1.5 wt.%, respectively, and may even reach the primary lead−zinc ore boundary grade [24−26]. However, the current research on the extraction and recovery of lead and zinc from copper slag primarily emphasizes leaching and reduction processes. Simultaneously, there is a scarcity of reports on behaviors of lead and zinc in copper slag depletion processes [27,28]. Therefore, it is essential to investigate the occurrence and distribution of lead and zinc in copper matte, depleted copper slag, and collected flue dust to facilitate the efficient recovery of lead and zinc during the depletion process of molten copper slag.

Based on this premise, the study focused on elucidating the enrichment behavior of copper, lead, and zinc under various depletion conditions. Moreover, it established a model detailing the interphase (matte, slag, gas) migration and enrichment of lead and zinc. This paper aims to guide the collaborative and energy-efficient recovery of valuable metals from copper slag in the smelting process.

2 Experimental

2.1 Material analysis

The chemical composition of the experimental copper slag from Guangxi, China, is presented in Table 1. The main components of copper slag are oxides of iron and silicon. Notably, the contents of copper and zinc in the copper slag are 2.63 wt.% and 1.24 wt.%, respectively.

The X-ray diffraction pattern of copper slag is depicted in Fig. 1. The primary mineral phases in copper slag are fayalite (Fe_2SiO_4) and magnetite (Fe_3O_4). No diffraction peaks were observed for

lead, zinc, and copper, likely due to their weak crystallinity and low concentration [29].

Copper slag was analyzed using electron probe micro-analysis (EPMA) to investigate its mineral phase structure, as presented in Fig. 2. The image reveals the presence of three distinct phases: the copper-rich phase delineated by the red dashed line, the irregular leaf-like structure phase indicated by the green dashed line, and a large-area base phase characterized by a rod-like structure. The base phase of copper slag is Fe_2SiO_4. The irregular leaf-like structure, marked by the green dashed line, primarily consists of an enrichment zone of Fe and O, devoid of silicon. A combined analysis of atomic ratios and XRD results identifies this phase as Fe_3O_4. The primary component within the red dashed line is copper sulfide (Cu_2S), which represents the copper matte phase. Lead is wrapped inside the copper matte, and zinc sulfide is located at the edge of the copper matte. These three substances exhibit immiscibility with each other and possess distinct interfaces. Furthermore, lead and zinc are dispersed on the surface of the copper slag.

Table 1 Chemical composition of experimental copper slag (wt.%)

Fe	Si	Cu	Al	Ca	Zn
41.93	11.66	2.63	1.21	1.98	1.24
Pb	As	Mo	S	O	
0.54	0.13	0.22	0.53	37.91	

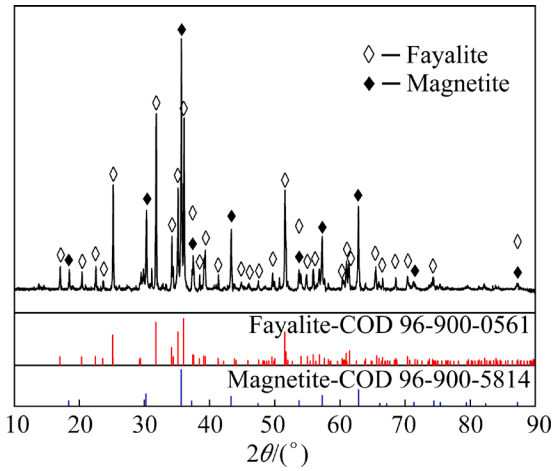

Fig. 1 XRD patterns of copper slag

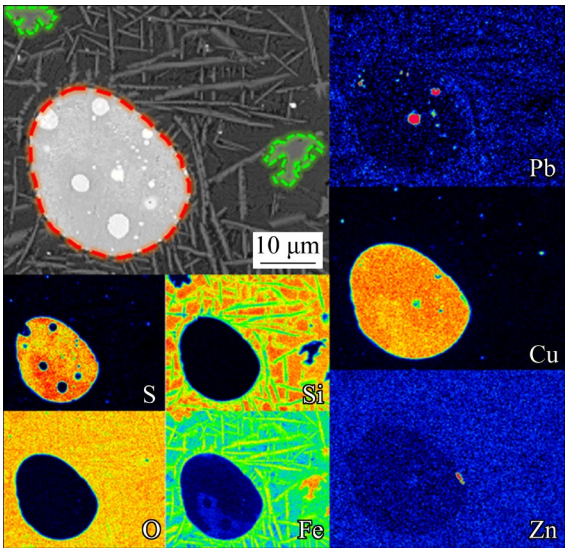

Fig. 2 EPMA surface scanning results of copper slag

A mineral liberation analyzer (MLA) was used to study the surface mineral composition of the copper slag, as shown in Fig. 3. Four mineral phases are found on the surface, which are fayalite (86.95 wt.%), magnetite (11.53 wt.%), chalcocite (Cu_2S, 1.19 wt.%), and domeykite (Cu_3As, 0.22 wt.%). Due to different degrees of agglomeration, the size

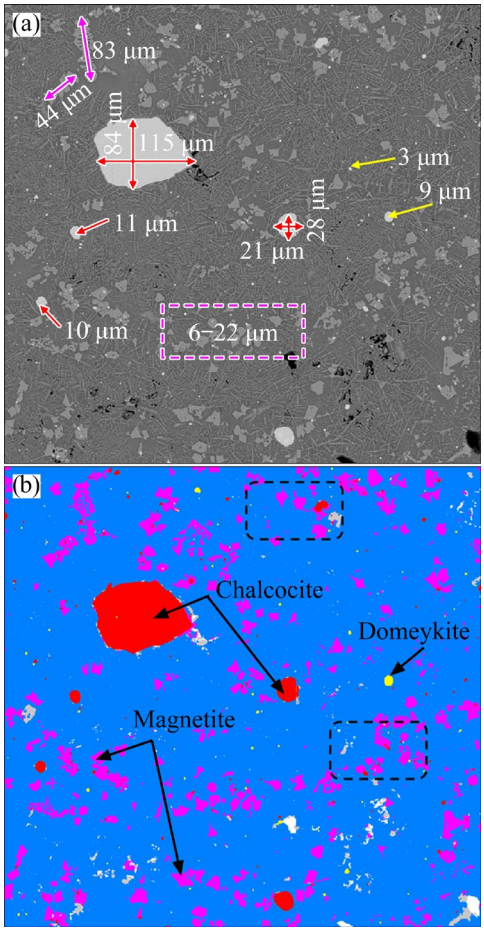

Fig. 3 Particle size (a) and distribution (b) of different mineral phases in copper slag

of Fe_3O_4 is 6−83 μm, as shown in Fig. 3(a). Cu_3As and Cu_2S have a maximum size of 9 and 115 μm, respectively, and their minimum sizes are less than 1 μm. Moreover, the tiny particles of Cu_2S and Cu_3As are disseminated in the black dot region of Fig. 3(b), with some being trapped and enveloped by the Fe_3O_4 phase. Unlike the EPMA results, no concentrated phases of lead and zinc are observed in the MLA results. Since MLA can only detect the phase composition of mineral surfaces, this may indicate that lead and zinc are encapsulated in the Fe_2SiO_4 phase.

2.2 Experimental methodology

The experimental equipment is a self-designed induction furnace with a stirring device [14]. The depletion experiment factors are shown in Table S1 of Supplementary Materials (SM). The calculation method for the copper recovery rate is illustrated as

$$\eta_{Cu}=\frac{M\alpha_{Cu}-m\beta_{Cu}}{M\alpha_{Cu}}\times 100\% \quad (1)$$

where α_{Cu} and β_{Cu} are copper contents in the slag before and after depletion, respectively, wt.%; m and M are the masses of copper slag before and after depletion, respectively, g; η_{Cu} is the copper recovery rate, %.

2.3 Analysis methods

The samples were characterized by X-ray diffraction analyzer (10 (°)/min, 2θ: 10°−90°, XRD, D8 Advance, Bruker, Germany) and operated at 40 kV and 40 mA with a Cu K_α radiation source. The resultant patterns were compared with the Joint Committee on Powder Diffraction Standards International Center for Diffraction Data (JXPDS-ICDD) database to identify the crystalline phases. The X-ray fluorescence analyzer (XRF, ZSX Primus IV, Rigaku Corporation, Tokyo, Japan) was used to qualitatively analyze the chemical composition of samples. Chemical analysis was used to analyze the composition of samples quantitatively. The electron microscope-microprobe analyzer (EPMA, JXA−8530F Plus, JEOL, Japan) was used to quantitatively analyze the microelement distribution of samples. The advanced mineral identification and characterization system (AMICS, Zeiss, Bruker, Germany) was used to quantitatively analyze the surface mineral distribution of samples.

3 Results and discussion

3.1 Thermodynamic analysis

The partial pressures of sulfur (S) and oxygen (O) in the gas phase were calculated at various temperatures using the FactSage Equilib program. The partial pressures are converted into corresponding logarithmic forms: sulfur and oxygen potential represented as *A*, *B*, *C*, and *D*, respectively. The findings are displayed in Fig. 4. Both the sulfur and oxygen potentials in copper slag exhibit an increasing trend with rising temperature.

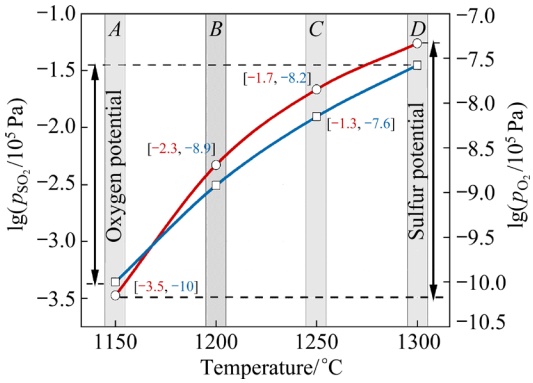

Fig. 4 Equilibrium phase showing sulfur and oxygen potential calculated based on copper slag composition

The predominance-area diagram for zinc and lead is illustrated in Fig. 5, generated using the FactSage Predom module. Four distinct equilibrium phases of zinc at various temperatures, oxygen, and sulfur potentials are illustrated in Fig. 5(a). Figure 5(b) illustrates five distinct equilibrium phases of lead at various temperatures, oxygen, and sulfur potentials. By incorporating the sulfur and oxygen potentials (*A*−*D*) of copper slag raw materials from Fig. 4 into the predominance- area diagram in Fig. 5, it is evident that zinc in copper slag primarily exists in the form of zinc oxide. Simultaneously, the presence of zinc sulfide in copper slag correlates with variations in smelting temperature. Lead in copper slag predominantly exists as an elementary substance.

The standard Gibbs free energy variations for Eqs. (2)−(14) were calculated using the FactSage Reaction program. The results and specific data are presented in Fig. 6 and Table S2 of SM, respectively.

At the depletion temperature, lead−zinc oxide can spontaneously convert to the corresponding sulfide when the sulfur potential reaches a certain

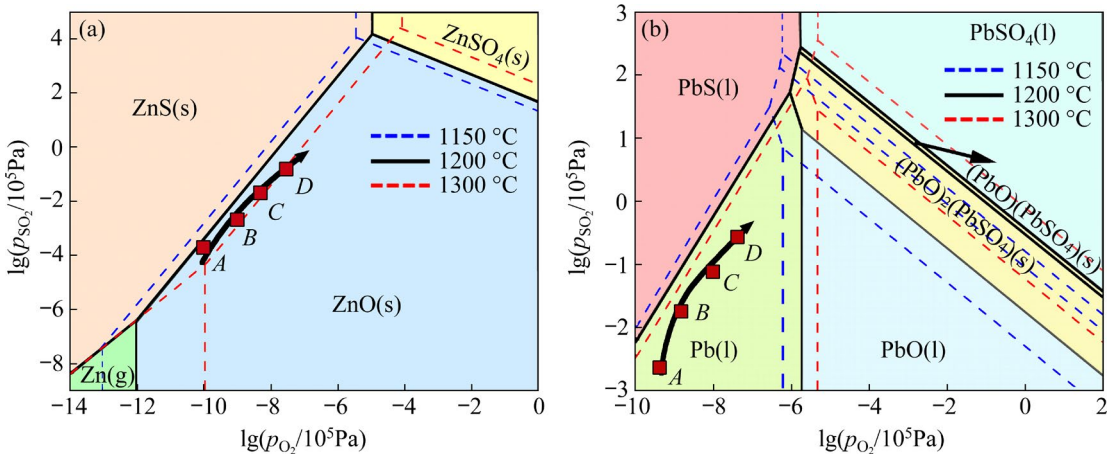

Fig. 5 Equilibrium predominance-area diagram of zinc (a) and lead (b) at different temperatures

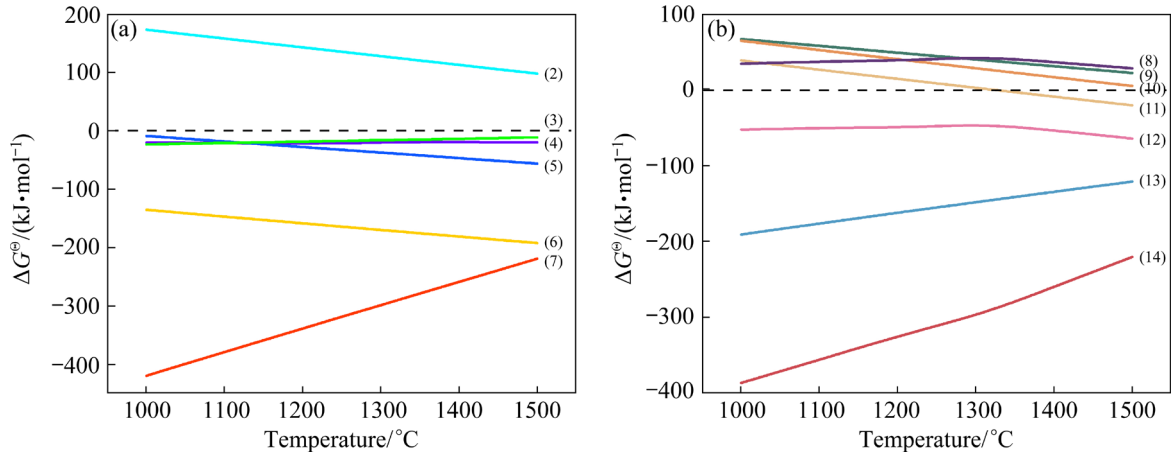

Fig. 6 Standard Gibbs free energy variation of for possible reactions zinc (a) and lead (b) compounds

level, as shown in Eqs. (4) and (9). The volatilization process of zinc sulfide under atmospheric pressure is challenging to proceed spontaneously, as shown in Eq. (2). Zinc exhibits higher volatility than zinc oxide under atmospheric pressure, and this trend becomes more pronounced with increasing temperature, as evidenced in Eqs. (3) and (5). Lead and lead oxide are not readily volatilized at the depletion temperature, as depicted in Eqs. (9) and (10). When the temperature exceeds 1278 °C, the spontaneous volatilization of lead sulfide occurs, as shown in Eq. (11). Elementary substance forms of lead and zinc are unstable and quickly transform into oxides [30], as outlined in Eqs. (7) and (13). Under high oxygen potential, lead sulfide can further convert into the corresponding sulfate, as indicated in Eq. (14).

$$ZnS(l)=ZnS(g) \quad (2)$$

$$ZnO(l)=ZnO(g) \quad (3)$$

$$ZnO+FeS=ZnS+FeO \quad (4)$$

$$Zn(l)=Zn(g) \quad (5)$$

$$ZnS+O_2=Zn+SO_2 \quad (6)$$

$$2Zn+O_2=2ZnO \quad (7)$$

$$Pb+FeS=PbS+FeO \quad (8)$$

$$Pb(l)=Pb(g) \quad (9)$$

$$PbO(l)=PbO(g) \quad (10)$$

$$PbS(l)=PbS(g) \quad (11)$$

$$PbO+FeS=PbS+FeO \quad (12)$$

$$2Pb+O_2=2PbO \quad (13)$$

$$PbS+2O_2=PbSO_4 \quad (14)$$

Equilibrium concentrations were calculated using FactSage 7.3 for various amounts of ferrous sulfide (FeS) additions. The calculation was performed under the following conditions: 100 g copper slag, 1200 °C, and 1×10^5 Pa. The calculation results are presented in Fig. 7, with further details available in Table S3 of SM. As the FeS addition

increases, the equilibrium concentration of zinc oxide decreases correspondingly, while zinc sulfide has the opposite effect. Under conditions of low sulfur potential, lead oxide is generated. As predicted by the thermodynamic calculations, the conversion of lead oxide into lead sulfide commences with an increase in sulfur potential. At higher sulfur potential levels, the oxygen in the cuprous oxide (Cu_2O) phase within the copper slag is progressively replaced by sulfur, resulting in the formation of the Cu_2S phase, which subsequently settles into the copper matte layer. Theoretically, all minute liquid droplets transforming from Cu_2O to Cu_2S can settle into the copper matte layer over a sufficient duration. However, even in the presence of a high sulfur potential within an open system, complete conversion of Cu_2O to Cu_2S is not achievable. It tends to reach a maximum conversion limit referred to as the depletion limit.

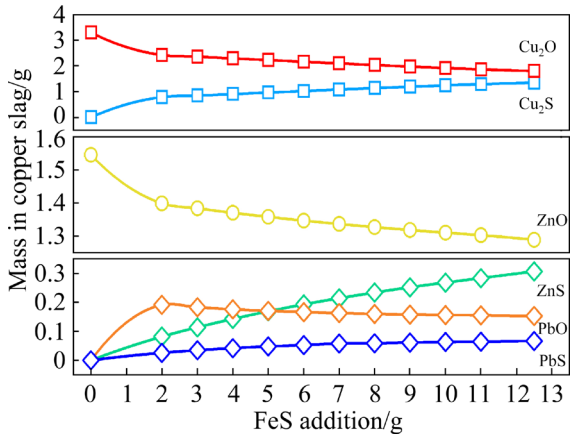

Fig. 7 Equilibrium mass under different FeS additions

The phase diagram of Fe−Ca−Si oxide ternary slag is shown in Fig. S1 of SM. The Point 8 is a three-phase eutectic point. When the temperature exceeds 1093.79 °C, the slag corresponding to this component presents a liquid-phase state. The eutectic point comprises 41.229 wt.% olivine phase, 14.087 wt.% tridymite phase, and 44.683 wt.% wollastonite phase.

3.2 Lead and zinc behaviors in depletion process

The copper slag and flux were mixed in the mixing tank with a mass ratio of 10:1. After the mixed material was melted in the induction furnace, stirring began at a speed of 100 r/min. The detailed experimental parameters and results are presented in Table S1 of SM and Fig. 8, respectively. As depicted in Fig. 8(a), the highest copper recovery rate is 87.83% at 1200 °C. Excessively low or high temperatures are not conducive to copper recovery. The elevated viscosity and limited fluidity of the molten slag at low temperatures hinder the settling of copper matte. The depletion reaction is intense at high temperatures, and the generated sulfur dioxide (SO_2) bubbles escape too quickly and carry copper matte into the slag phase. The trends in the variation of lead and zinc contents in the depleted copper slag are consistent with the theoretical calculations presented in Fig. 6. When FeS addition is 3 wt.%, the recovery rate of copper reaches a maximum of 87.83%, as shown in Fig. 8(b). No significant change in the copper recovery rate or the lead and zinc content of the slag with various amounts of FeS addition, which is also the conclusion of the theoretical calculation in Fig. 7. As shown in Fig. 8(c), the lead and zinc content in the depleted copper slag shows a downward trend. The Fe/SiO_2 mass ratio of 1.0 corresponds precisely to the lowest liquid phase region (Point 8) in Fig. S1 of SM, when the minimum melting temperature of the slag is 1093.79 °C. An excessively low or high Fe/SiO_2 mass ratio will elevate the liquid phase temperature and slag viscosity, thereby impacting the settling rate of copper matte. The smelting time has a limited impact on the lead and zinc content in the depleted copper slag, as shown in Fig. 8(d). The copper achieves a peak recovery rate of 90.13% within less than 45 min. The spontaneous volatilization of zinc sulfide, lead sulfide, lead, and lead oxide at the depletion temperature, as depicted in Fig. 6, is challenging to achieve. While zinc and zinc oxide can theoretically volatilize, there remains a high concentration of lead and zinc in the slag. Therefore, it is concluded that most of the lead-containing phase and some of the zinc-containing phase enter the matte phase through the sedimentation process, and most of the zinc-containing phase is wrapped in the slag by the Fe_2SiO_4 phase or other mineral phases.

3.3 Distribution and migration mechanism of lead−zinc multiphase

The distribution results of lead and zinc in slag, matte, and gas phases are presented in Tables S4−S6 of SM. The copper contents in the copper slag and copper matte phases, after depletion and

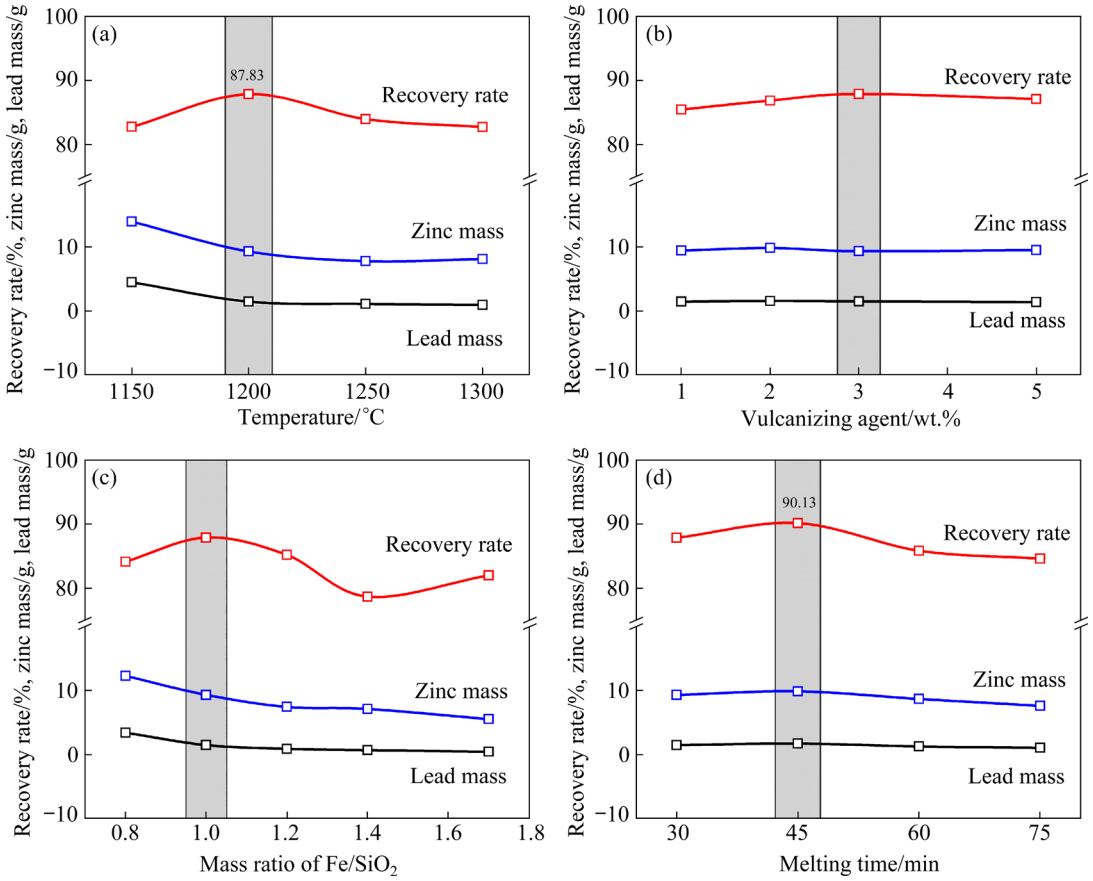

Fig. 8 Variation of copper recovery rate with temperature (a), vulcanizing agent (b), mass ratio of Fe/SiO_2 (c), and melting time (d)

enrichment, are 0.22 wt.% and 28.89 wt.%, respectively. Additionally, the distribution of other valuable elements was investigated and presented in Fig. 9 and Table S7 of SM.

The lead content in the collected flue dust is 54.07 wt.%, while the zinc content is comparatively lower at 17.42 wt.%. It suggests a weaker migration activity of zinc during the depletion process, which may be attributed to the substitution of some Fe atoms by Zn in the Fe_2SiO_4, forming a zinc-rich olivine phase. The difficulty in decomposing the Fe_2SiO_4 phase during depletion hinders the release and volatilization of zinc. The distribution of sulfur in depleted copper slag and copper matte is similar, and arsenic mainly exists in collected flue dust and copper matte phases.

The X-ray diffraction results for the three different products are illustrated in Fig. 10. The main phases in the flue dust are lead sulfate and zinc oxide, while in the depleted slag, the predominant phase is Fe_2SiO_4. The presence of $CaMg(SiO_3)_2$ is related to the added calcium oxide flux. The primary phases in the copper matte are

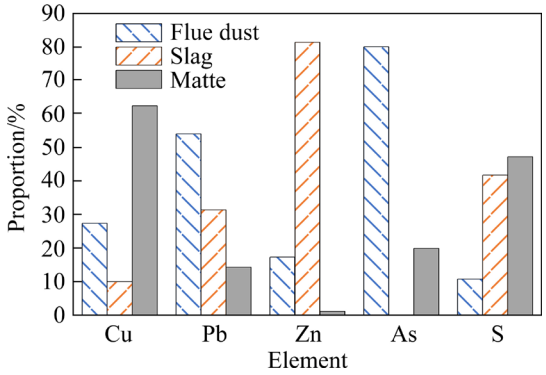

Fig. 9 Multi-element distribution of depleted copper slag, copper matte, and collected flue dust

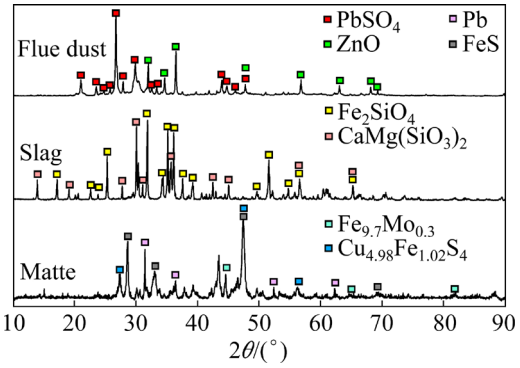

Fig. 10 XRD patterns of three phases

ferrous sulfide, $Cu_{4.98}Fe_{1.02}S_4$, and $Fe_{9.7}Mo_{0.3}$. The crystallinity and mineral content significantly impact the X-ray diffraction results, posing challenges in using X-ray diffraction alone to determine every mineral phase. Therefore, a more comprehensive analysis of depleted copper slag, copper matte, and collected flue dust was conducted using EPMA, with the results depicted in Figs. 11 and 12.

The EMPA micrographs and point scanning positions of copper slag are depicted in R-1−R-4 in Fig. 11. FD-1 and FD-2 are microscopic images of different locations of collected flue dust. Multi-element energy spectrum results for the corresponding positions of the copper slag and collected flue dust are provided in Table S8 of SM.

Fe_2SiO_4 is the base phase of the copper slag raw material (Points 3 and 5). It is mixed with other elements, such as lead and zinc, to create a novel dendritic olivine phase (Points 7 and 8). Further-

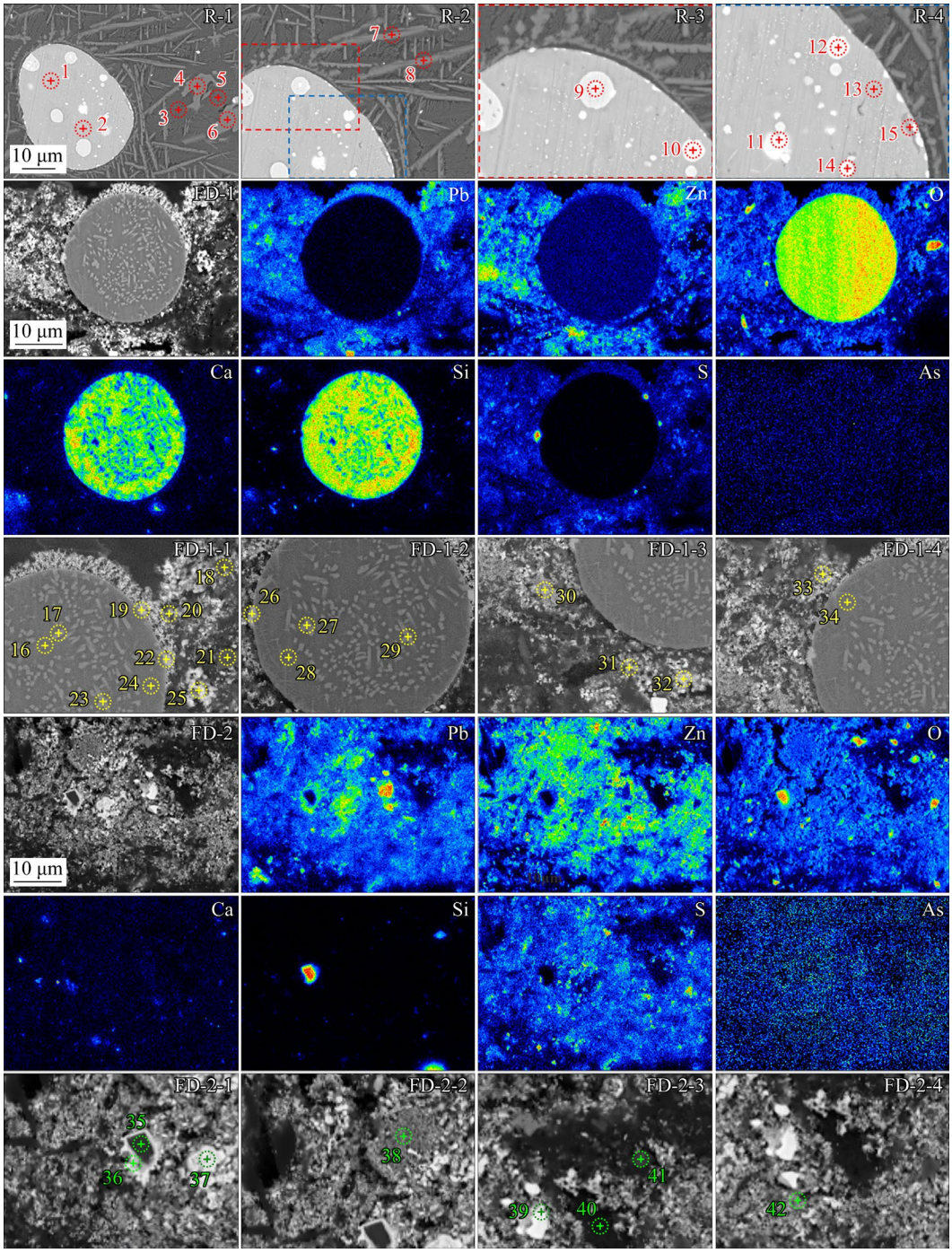

Fig. 11 Point scan position and area scan distribution results of copper slag (R) and collected flue dust (FD) samples

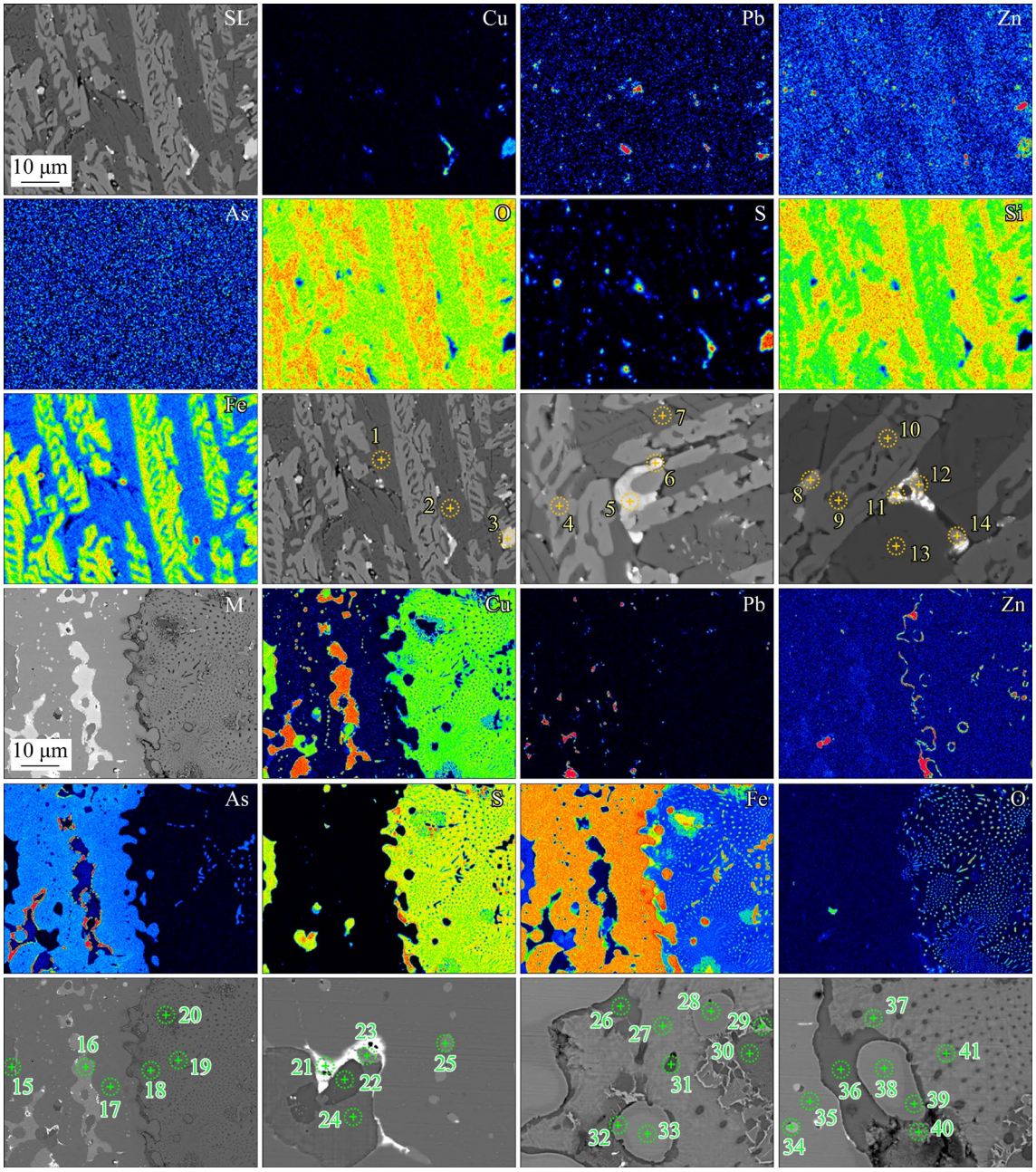

Fig. 12 Point scan position and area scan distribution results of depleted copper slag (SL) and copper matte (M) samples

more, an intercalation relationship exists between Fe_2SiO_4 and some larger particles of copper matte which are either wholly or partially encapsulated by Fe_2SiO_4 (Points 1, 2, 7 and 8). Additionally, a flower-like Fe_3O_4 phase typically surrounds the copper matte (Points 4 and 6). Consequently, the Fe_3O_4 phase significantly influences the settling of copper matte within copper slag. In addition, small copper matte particles are discovered within the dendritic Fe_2SiO_4 structure of the base phase. An amplification analysis of copper matte in copper slag raw materials reveals that the edges of copper matte particles are slightly enriched in zinc sulfide and lead sulfide (Points 11, 12 and 15). Lead is enclosed within the copper matte and exists as elementary substance (Points 10, 11, 12 and 14). Arsenic in the copper matte reacts with copper to form the Cu_3As phase (Points 9, 10 and 14). Cu_2S and FeS (Points 1 and 2) are the fundamental phases of the copper matte, as determined by X-ray diffraction findings.

In the collected flue dust, lead is primarily present in the form of lead sulfate (as indicated by Points 18, 20 and 22), with a minor presence of lead sulfide (evidenced by Points 30 and 31). Zinc predominantly exists as zinc oxide (refer to Points

25, 32 and 33). Notably, arsenic in the collected flue dust exhibits poor crystallinity, mainly occurring in an amorphous state, and this is why the characteristic diffraction peaks of arsenic are not discernible in Fig. 10. The primary arsenic compounds in the collected flue dust are arsenic oxide (As_2O_3) and arsenate (as indicated by Points 20, 25, 32 and 37). Copper is present in the collected flue dust in two primary forms: Cu_2S and copper sulfate ($CuSO_4$) (as indicated by Points 19 and 26). Furthermore, the predominant iron compounds in the collected flue dust are Fe_3O_4 and Fe_2SiO_4 (refer to Points 27, 28 and 29). This association is linked to the ability of the slag to transport gas, particularly the SO_2 gas generated during depletion, which carries tiny droplets of slag into the collected flue dust.

The multi-element energy spectrum and point analysis results are depicted in Fig. 12 and Table S9 of SM. The base phase in the depleted copper slag is Fe_2SiO_4 (Points 1, 2 and 4). The lead primarily exists in the form of elementary substance and lead sulfide in the incompletely settled copper matte particles within the depletion slag (Point 11). The zinc is primarily associated with the Fe_2SiO_4 phase. The absence of irregular leaf-like structures in the depleted slag signifies a notable reduction in the Fe_3O_4 phase due to the addition of FeS. Additionally, agitation expedites the collision and directed settling of small copper matte particles in the depleted slag.

In copper matte, lead is wrapped in its elementary substance form (Points 21 and 23), while zinc exists in the form of zinc sulfide at the periphery of the copper matte (Points 22 and 26). The primary phase of copper in the copper matte is Cu_2S (Points 15, 19 and 24), with trace amounts of metallic copper (Points 16, 23 and 25). Iron in the copper matte is present in the forms of Fe, FeS and Fe_3O_4 (Points 20, 21, 24, 27 and 28). Additionally, arsenic aggregates in the copper matte are predominantly in the form of Cu_3As phase (Points 33, 34, 35 and 38).

A model for the interphase migration of lead and zinc during the depletion process was proposed, as depicted in Fig. 13. The occurrence phase transformation of zinc during the direct depletion of copper slag mainly includes two steps: (1) Zinc

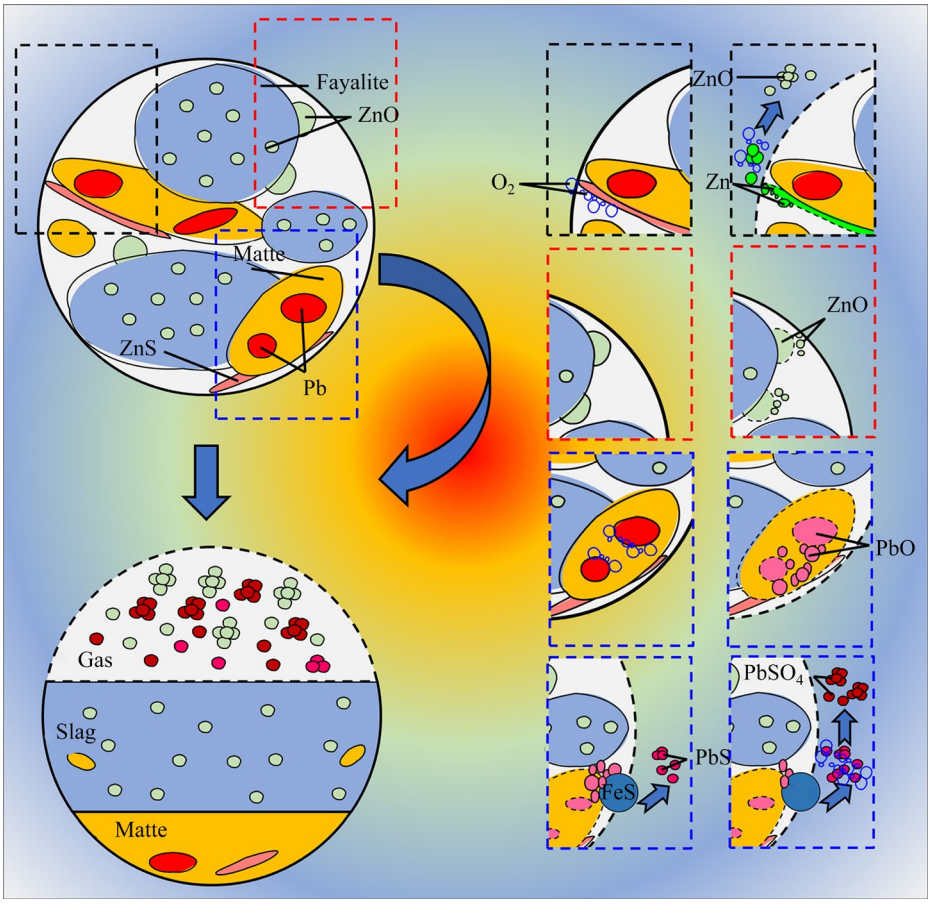

Fig. 13 Evolution model of lead−zinc occurrence patterns

oxide present in the interstitial sites of Fe_2SiO_4 volatilizes directly into the flue dust; (2) The zinc sulfide present at the boundary of the copper matte is oxidized to high-temperature zinc vapor by contacting oxygen in the air and volatilizes in the open system. When the high-temperature zinc vapor contacts the air, it is oxidized to zinc oxide immediately. The interphase migration process of lead includes three steps: (1) In the open system, the elementary substance lead in the copper matte is oxidized to lead oxide; (2) Under the participation of the FeS, lead oxide turns into lead sulfide and volatilizes into the flue dust; (3) The PbS-containing flue dust, when exposed to the air, is rapidly oxidized to lead sulfate. Therefore, the final lead is in the form of lead sulfate, lead sulfide in the flue dust, and lead in the copper matte phase. Most of the zinc is encapsulated in the Fe_2SiO_4 phase. The remaining zinc that Fe_2SiO_4 does not encapsulate is present in the flue dust phase as zinc oxide after two stages of oxidation.

4 Conclusions

(1) The primary mineral phases in copper slag are fayalite (86.95 wt.%), magnetite (11.53 wt.%), chalcocite (1.19 wt.%), and domeykite (0.22 wt.%). The fine particles of chalcocite and domeykite exhibit a dispersed distribution, some of which are wrapped by magnetite.

(2) Under the conditions of 1200 °C, a Fe/SiO_2 mass ratio of 1.0, 3 wt.% ferrous sulfide, and a duration of 45 min, copper achieves a recovery rate of 90.13%.

(3) During the depletion process, zinc undergoes interphase migration through the direct volatilization of zinc oxide, the sequential oxidation, and volatilization of zinc sulfide, accumulating in the flue dust in the form of zinc oxide. Lead undergoes interphase migration involving three steps: oxidation, sulfidation, and secondary oxidation. It accumulates in the flue dust in the form of lead sulfate.

CRediT authorship contribution statement

Jun HAO: Experiment, Data curation, Writing − Original draft, Writing – Review & editing; **Zhi-he DOU:** Experiment, Data curation, Writing − Original draft, Writing − Review & editing; **Xing-yuan WAN:** Software, Revision; **Ting-an ZHANG:** Adviser; **Kun WANG:** Adviser and revision.

Declaration of competing interest

The authors declare that they have no known competing financial interests or personal relationships that could have appeared to influence the work reported in this paper.

Acknowledgments

This work was supported by the Fundamental Research Funds for Central Universities, China (No. N2025004), the National Natural Science Foundation of China (Nos. U2102213, U1702253, 52204419), Major Science and Technology Project of Liaoning Province, China (No. 2021JH1/10400032), Major Science and Technology Project of Guangxi Province, China (No. 2021AA12013), and Liaoning Natural Science Foundation, China (No. 2022-BS-076).

Supplementary Materials

Supplementary Materials in this paper can be found at: http://tnmsc.csu.edu.cn/download/22-p3029-2023-0347-Supplementary_Materials.pdf.

References

[1] ERDENEBOLD U, CHOI H M, WANG J P. Recovery of pig iron from copper smelting slag by reduction smelting [J]. Archives of Metallurgy and Materials, 2018, 63: 1793−1798.

[2] TIAN Hong-yu, GUO Zheng-qi, PAN Jian, ZHU De-qing, YANG Cong-cong, XUE Yu-xiao, LI Si-wei, WANG Ding-zheng. Comprehensive review on metallurgical recycling and cleaning of copper slag [J]. Resources Conservation & Recycling, 2021, 168: 105366.

[3] PHIRI T C, SINGH P, NIKOLOSKI A N. The potential for copper slag waste as a resource for a circular economy: A review — Part I [J]. Minerals Engineering, 2022, 180: 107474.

[4] LIU Zhi-hong, XIA Long-gong. The practice of copper matte converting in China [J]. Mineral Processing and Extractive Metallurgy Review, 2019, 128: 117−124.

[5] KUIPERS K J J, van OERS L F C M, VERBOON M, VAN DER VOET E. Assessing environmental implications associated with global copper demand and supply scenarios from 2010 to 2050 [J]. Global Environmental Change, 2018, 49: 106−115.

[6] VELENTURF A P M, ARCHER S A, GOMES H I, CHRISTGEN B, LAG-BROTONS A J, PURNELL P. Circular economy and the matter of integrated resources [J]. Science of the Total Environment, 2019, 689: 963−969.

[7] ELSHKAKI A, GRAEDEL T E, CIACCI L, RECK B K. Copper demand, supply, and associated energy use to 2050 [J]. Global Environmental Change, 2016, 39: 305−315.

[8] SARFO P, DAS A, WYSS G, YOUNG C. Recovery of metal values from copper slag and reuse of residual secondary slag [J]. Waste Management, 2017, 70: 272−281.

[9] ZHANG Hui-bin, WANG Ya-nan, ZHU Yin-bin, REN Peng, HU Bin, XU Sheng-hang, CAO Hua-zhen, ZHOU Jun, ZHENG Guo-qu. Determination of occurrence and leaching toxicity of arsenic in copper flash smelting slags [J]. Transactions of Nonferrous Metals Society of China, 2023, 33: 293−303.

[10] LI Yuan, JI Li, MI Wu-juan, XIE Shu-lian, BI Yong-hong. Health risks from groundwater arsenic on residents in Northern China coal-rich region [J]. Science of the Total Environment, 2021, 773: 145003.

[11] CAPPUYNS V, ALIAN V, VASSILIEVA E, SWENNEN R. pH dependent leaching behavior of Zn, Cd, Pb, Cu and As from mining wastes and slags: kinetics and mineralogical control [J]. Waste and Biomass Valorization, 2014, 5: 355−368.

[12] POTYSZ A, KIERCZAK J, PIETRANIK A, KĄDZIOŁKA K. Mineralogical, geochemical, and leaching study of historical Cu-slags issued from processing of the Zechstein formation (Old Copper Basin, southwestern Poland) [J]. Applied Geochemistry, 2018, 98: 22−35.

[13] XU Da-mao, FU Rong-bing, TONG Yun-hua, SHEN Dao-lu, GUO Xiao-pin. The potential environmental risk implications of heavy metals based on their geochemical and mineralogical characteristics in the size-segregated zinc smelting slags [J]. Journal of Cleaner Production, 2021, 315: 128199.

[14] KAKSONEN A H, SÄRKIJÄRVI S, PEURANIEMI E, JUNNIKKALA S, PUHAKKA J A, TUOVINEN O H. Metal biorecovery in acid solutions from a copper smelter slag [J]. Hydrometallurgy, 2017, 168: 135−140.

[15] HAO Jun, DOU Zhi-he, ZHANG Ting-an, JIANG Bao-cheng, WANG Kun, WAN Xing-yuan. Manufacture of wear-resistant cast iron and copper-bearing antibacterial stainless steel from molten copper slag via vortex smelting reduction [J]. Journal of Cleaner Production, 2022, 375: 134202.

[16] PHIRI T C, SINGH P, NIKOLOSKI A N. The potential for copper slag waste as a resource for a circular economy: A review — Part II [J]. Minerals Engineering, 2021, 172: 107150.

[17] WANG Zeng-wu, GAO Jin-tao, LAN Xi, FENG Guo-liang, GUO Zhan-cheng. A new method for continuous recovery of fine copper droplets from copper matte smelting slag via super-gravity [J]. Resources, Conservation & Recycling, 2022, 182: 106316.

[18] POOJA G, KUMAR P S. Various surface-active agents used in flotation technology for the removal of noxious pollutants from wastewater: A critical review [J]. Environmental Science: Water Research & Technology, 2023, 9: 994−1007.

[19] LI Si-wei, PAN Jian, ZHU De-qing, GUO Zheng-qi, XU Ji-wei, CHOU Jian-lei. A novel process to upgrade the copper slag by direct reduction-magnetic separation with the addition of Na_2CO_3 and CaO [J]. Powder Technology, 2019, 347: 159−169.

[20] YUAN Shuai, ZHOU Wen-tao, HAN Yue-xin, LI Yan-jun. Selective enrichment of iron particles from complex refractory hematite-goethite ore by coal-based reduction and magnetic separation [J]. Powder Technology, 2020, 367: 305−316.

[21] WANG Lin-song, GAO Zhi-yong, TANG Hong-hu, WANG Li, HAN Hai-sheng, SUN Wei, QU Yong-bao, YANG Yue. Copper recovery from copper slags through flotation enhanced by sodium carbonate synergistic mechanical activation [J]. Journal of Environmental Chemical Engineering, 2022, 10: 107671.

[22] ZHANG Si-hai, ZHU Neng-wu, MAO Fu-lin, ZHANG Jian-yi, HUANG Xi-xian, LI Fei, LI Xin-yu, WU Ping-xiao, DANG Zhi. A novel strategy for harmlessness and reduction of copper smelting slags by alkali disaggregation of Fe_2SiO_4 coupling with acid leaching [J]. Journal of Hazardous Materials, 2021, 402: 123791.

[23] HU Ying-yan, LI Ming, WU Wei-guo, KE Yong, LIU Lu-jing, WANG Xue-liang. Life cycle assessment for waste acid treatment in zinc smelting [J]. Transactions of Nonferrous Metals Society of China, 2022, 32: 3822−3834.

[24] ZHANG Bei-kai, WANG Qin-meng, GUO Xue-yi, TIAN Qing-hua. Mechanism and kinetics for chlorination roasting of copper smelting slag [J]. Transactions of Nonferrous Metals Society of China, 2023, 33: 563−575.

[25] CHEN Yu-jie, ZHAO Zong-wen, TASKINEN P, LIANG Yan-jie, OUYANG Hong-chuan, PENG Bing, JOKILAAKSO A, ZHOU Song-lin, CHEN Tao, PENG Ning, LIU Hui. Characterization of copper smelting flue dusts from a bottom-blowing bath smelting furnace and a flash smelting furnace [J]. Metallurgical and Materials Transactions B-Process Metallurgy and Materials Processing Science, 2020, 51: 2596−2608.

[26] LI Zhong-chen, TIAN Qing-hua, WANG Qin-meng, GUO Xue-yi. Recovery of copper, lead and zinc from copper flash converting slag by the sulfurization-reduction process [J]. JOM, 2023, 75(4): 1107−1118.

[27] ZHANG Bei-kai, GUO Xue-yi, WANG Qin-meng, TIAN Qing-hua. Thermodynamic analysis and process optimization of zinc and lead recovery from copper smelting slag with chlorination roasting [J]. Transactions of Nonferrous Metals Society of China, 2021, 31: 3905−3917.

[28] ZHANG Qian, FENG Qi-cheng, WEN Shu-ming, CUI Chuan-fa, LIU Jun-bo. A novel technology for separating copper, lead and zinc in flotation concentrate by oxidizing roasting and leaching [J]. Processes, 2019, 7: 376.

[29] HUANG X H. Principles on ferrous metallurgy [M]. Beijing: Metallurgical Industry Press, 2013. (in Chinese)

[30] LI H G. Metallurgical principle [M]. Beijing: Science Press, 2005. (in Chinese)

铜渣贫化过程中铅和锌的相间迁移和富集

郝 君[1,2]，豆志河[1,2]，万兴元[1,2]，张廷安[1,2]，王 坤[1,2]

1. 东北大学 多金属共生矿冶金教育部重点实验室，沈阳 110819；
2. 东北大学 冶金学院，沈阳 110819

摘 要：建立铅和锌在熔融铜渣贫化过程中不同物相间的迁移和富集规律模型。通过硫氧势图计算预测铜渣中不同组分的赋存状态，并通过高温实验进行了验证。在 1200 °C、当铁硅质量比 1.0，硫化亚铁 3%(质量分数)、熔炼时间 45 min 的条件下，铜回收率可达 90.13%。铅(54.07%，质量分数)和锌(17.42%，质量分数)以硫酸铅、硫化铅和氧化锌的形式进入烟尘，并以铅单质(14.44%，质量分数)和硫化锌(1.29%，质量分数)的形式进入铜锍。剩余的铅和锌以氧化物的形式被包裹在铁橄榄石相中。

关键词：贫化；铅；铜渣；搅拌；锌

(Edited by Xiang-qun LI)